Turkish Journal of Electrical Engineering & Computer Sciences

http://journals.tubitak.gov.tr/elektrik/

Research Article

Turk J Elec Eng & Comp Sci
(2018) 26: 1623 – 1637

doi:10.3906/elk-1709-101

Model predictive control of a dual induction motor drive fed by a single voltage source inverter

Muhammad Abbas ABBASI[1,2,*], **Abdul Rashid BIN HUSAIN**[1]

[1]Department of Robotics & Control, Faculty of Electrical Engineering, Universiti Teknologi Malaysia, Skudai, Malaysia

[2]Department of Electronic Engineering, The Islamia University of Bahawalpur, Bahawalpur, Pakistan

Received: 12.09.2017 • **Accepted/Published Online:** 03.04.2018 • **Final Version:** 30.05.2018

Abstract: In dual induction motor control applications, averaging of controlled variables, mean circuit models, or master/slave strategies are used, which lead to unbalanced and unstable operation of the overall drive system. An improved finite control set predictive torque control (FCS-PTC) method is proposed for the parallel operation of two induction motors. The optimization cost function of the controller is shown to meet multiple objectives simultaneously, eliminating the use of averaging techniques and without leading to unbalanced conditions. The simulation results are compared with direct torque control (DTC) for dual induction motors. As compared to DTC, model predictive control shows low torque and flux ripple, 5% lower current THD, improved current balancing between the motors, and negligible effect of parameter mismatch.

Key words: Model predictive control (MPC), dual induction motor drive, predictive torque control, voltage source inverter (VSI), induction motor

1. Introduction

Induction motors are extensively used in different industries and have almost completely replaced DC motors, owing to their excellent performance, ruggedness, reliability, and almost maintenance-less operation [1–3]. Multiple induction motors fed by a single power converter are also used in numerous applications such as extruder mills, conveyers, steel processing, aerospace, tanks, and locomotive tractions [1]. Parallel induction motors are fed by a single converter because of the simple configuration, smaller size of the setup, and low cost.

However, there are certain challenges and issues involved in the parallel operation of induction motors. The motors must be identical with equal power ratings if they are being fed by a single inverter. For example, if two induction motors are being used in locomotive traction where each motor usually drives an axle of a wheel, then these motors must be matched for speed-torque characteristics and run at the same speed to avoid slippage or skidding [4]. If motors do not share identical torque-speed characteristics, then the inverter will see unequal impedances and currents flowing through each motor will be different. Eventually load torque sharing, in such situations, will also be different [4–6].

In industrial applications of induction motors, mostly PI controllers coupled with PWM and hysteresis controllers are used [7,8]. Generally, field oriented control (FOC) dominates as the control strategy of choice for

*Correspondence: abbas.abbasi@iub.edu.pk

higher performance drives. Other advanced techniques include direct torque control (DTC), model predictive control (MPC), fuzzy logic control, sliding mode control, and neural networks among others [9,10].

However, for parallel operation of induction motors, these conventional methods become tedious and difficult to implement. For example, in FOC control of parallel induction motors, it becomes cumbersome to achieve field orientation for several machines at the same time using a single controller [5,9]. Therefore, to implement FOC or vector control to such systems, the overall system is considered as a single large motor based on two principles [5]: either all the connected induction motors are used to take the average of measurements for feedback loop, or a master/slave concept is used to select one motor as the master and the others to follow it. However, such techniques ignore the characteristics mismatch such as slip difference among the motors. Other techniques, such as DTC, also use average circuit models or average measurements to treat the system as a single induction motor and hence the problem of characteristic mismatch and parameter variation is also affected adversely in the implementation of such controllers. Such problems can be overcome by the use of model predictive control (MPC) [7,11].

MPC is ideally suited for the control of dual induction motors since it can control all the parallel connected motors without considering the average circuit model or master/slave configuration [11–14]. Load sharing between the dual induction motors, current balance, torque sharing, and flux control of individual motor becomes an easy task that can be achieved by introducing the control objective into the cost function of the controller. MPC discussed in this paper uses a simple configuration with a three-phase voltage source inverter and demonstrates its effectiveness in dealing with different challenges involved in dual motor drive control. It employs the techniques developed in [6,7] and extends the formulation of the controller to include various features such as implementation of initial current constraints, load sharing, tuning of the speed regulation loops for both motors, model uncertainties in the controller, effect of parameter variations on load sharing, and flux variations due to mismatched characteristics. Proposed controller cost functions take measurements from both of the motors and do not average out the circuit, hence not compromising on the nonlinearities involved in the system. Taking into account the operating conditions of all the motors, safety is guaranteed.

The paper is organized as follows: Sections 2 and 3 present the mathematical models of the dual induction motor drive and the inverter suitable for the implementation of MPC. Section 4 deals with detailed MPC design method, cost function formulation, estimation, prediction, and optimization. Finally section 5 discusses some simulation results to validate the usefulness of the controller design.

2. Modelling dual induction motor drive system

A dual induction motor drive fed by a three-phase voltage source inverter is shown in Figure 1 [1,12]. A constant dc source V_{dc} is assumed to be feeding the inverter. This voltage can be obtained from the line power using a power converter. The inverter provides phase currents i_a, i_b and i_c, which are divided between the stators of the two motors. For a stable operation, $i_{x1} = i_{x2}$, where $x = \{a, b, c\}$. However, due to the unavoidable phenomenon of parameter variations and mismatch between the motors, this condition is never actually met. MPC can directly manipulate the inverter switching states to minimize the difference between these currents, i.e. [7,15]

$$\begin{aligned} &Minimize \quad \Delta i_x = |i_{x1} - i_{x2}| \\ &Subject\ to\ \max\left(I_x\_initial\right) < I\_\lim \end{aligned}, \tag{1}$$

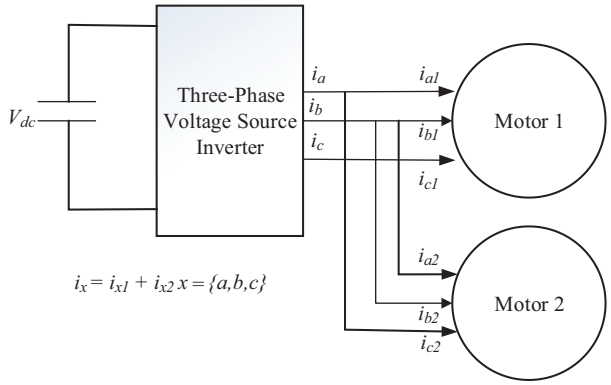

Figure 1. Dual induction motor drive fed by a three-phase voltage inverter.

where I_lim is the limit on any phase current during start-up. The dynamic model to design the MPC for dual induction motor is based on the discussion given in [12]. We will extend the model to two parallel connected motors sharing the same voltage at the same frequency.

Three-phase stator currents for the motors M1 and M2 can be defined in a fixed coordinate frame as follows [1,11,16]:

$$i_{a1} = I_{m1}.\sin(\omega_e t) \qquad i_{a2} = I_{m2}.\sin(\omega_e t) \tag{2}$$

$$i_{b1} = I_{m1}.\sin\left(\omega_e t - \frac{2\pi}{3}\right) \qquad i_{b2} = I_{m2}.\sin\left(\omega_e t - \frac{2\pi}{3}\right) \tag{3}$$

$$i_{c1} = I_{m1}.\sin\left(\omega_e t - \frac{4\pi}{3}\right) \qquad i_{c2} = I_{m2}.\sin\left(\omega_e t - \frac{4\pi}{3}\right), \tag{4}$$

where I_{m1} and I_{m2} represent peak currents in the two stators (assumed equal for a balanced condition) and ω_e is electrical frequency in rad/s. Stator currents can also be expressed in a two-coordinate complex reference frame (also known as $\alpha\beta$ frame) as

$$i_{s1} = \frac{2}{3}\left(i_{a1} + i_{b1}e^{j\frac{2\pi}{3}} + i_{c1}e^{j\frac{4\pi}{3}}\right) \qquad i_{s2} = \frac{2}{3}\left(i_{a2} + i_{b2}e^{j\frac{2\pi}{3}} + i_{c2}e^{j\frac{4\pi}{3}}\right) \tag{5}$$

In a similar fashion, equations of induction motors can be represented in any arbitrary complex reference frame rotating at an angular frequency ω_k. The variable ω in the following equations represents rotor speed and two sets of equations can be obtained for $i = 1, 2$. (Note that $v_{s1} = v_{s2}$ and the rotor is short circuited for both of the motors) [16].

$$v_s = R_{si}i_{si} + \frac{d\varphi_{si}}{dt} + j\omega_k\varphi_{si} \tag{6}$$

$$0 = R_{ri}i_{ri} + \frac{d\varphi_{ri}}{dt} + j(\omega_k - \omega)\varphi_{ri} \tag{7}$$

$$\varphi_{si} = L_{si}i_{si} + L_{mi}i_{ri} \tag{8}$$

$$\varphi_{ri} = L_{ri}i_{ri} + L_{mi}i_{si} \tag{9}$$

$$T_i = \frac{3}{2} pIm\left(\bar{\varphi}_{si} i_{si}\right) = -\frac{3}{2} pRe\left(\bar{\varphi}_{ri} i_{ri}\right), \tag{10}$$

where

- L_{si}, L_{ri} and L_{mi} are stator, rotor and mutual inductances in motor 1 and motor 2
- R_{si} and R_{ri} are stator and rotor resistances
- v_s and i_{si} are stator voltage and current vectors
- φ_{si} and φ_{ri} are stator and rotor flux vectors and $\bar{\varphi}$ represents complex conjugate
- T_i and p denote electromagnetic torques and number of pole pairs in induction motor (assumed equal for both motors)
- ω_k is the frequency of the rotating reference frame

Moreover,

$$J_i \frac{d\omega_{mi}}{dt} = T_i - T_{li} \tag{11}$$

$$\omega_i = p\omega_{mi} \tag{12}$$

J, T_l and ω_m are moment of inertia, load torque and angular mechanical speed of motors.

Eqs. (6) through (9) can easily be manipulated to produce the following state space model of the dual induction motor drive ($i = 1, 2$) [16]:

$$\tau_{\sigma i} \frac{di_{si}}{dt} = -i_{si} - j\omega_k \tau_{\sigma i} i_{si} + \frac{k_{ri}}{R_{\sigma i}} \left(\frac{1}{\tau_{\sigma i}} - j\omega_i \right) \varphi_{ri} + \frac{v_s}{R_{\sigma i}} \tag{13}$$

$$\tau_{ri} \frac{d\varphi_{ri}}{dt} = -\varphi_{ri} - j\left(\omega_k - \omega_i\right) \tau_{ri} \varphi_{ri} + L_{mi} i_{si} \tag{14}$$

Definitions of the various constants used in the above equations are given below:

$$\tau_{si} = \frac{L_{si}}{R_{si}}, \quad \tau_{ri} = \frac{L_{ri}}{R_{ri}} \tag{15}$$

$$\sigma_i = 1 - \frac{L_{mi}^2}{L_{si} L_{ri}}, \quad \tau_{\sigma i} = \frac{\sigma_i L_{si}}{R_{\sigma i}} \tag{16}$$

$$k_{ri} = \frac{L_{mi}}{L_{ri}}, \quad k_{si} = \frac{L_{mi}}{L_{si}} \tag{17}$$

$$R_{\sigma i} = R_{si} + R_{ri} k_{ri}^2 \tag{18}$$

Eqs. (13) and (14) will be used in the proposed controller to estimate rotor and stator flux and to predict stator currents, flux, and torque after discretization.

3. Inverter model

The three-phase voltage source inverter is shown in Figure 2. A constant voltage source V_{dc} is feeding the inverter. The constant voltage can be obtained from line voltage by using a suitable configuration of rectifier. The converter switches are operated in bipolar mode, i.e. no two switches in the same leg are turned on or off at the same time; therefore, a negation sign is shown on the switch logic symbols [16].

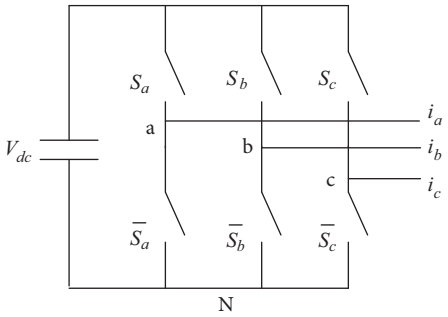

Figure 2. Simplified diagram of the three-phase voltage source inverter.

The switch logic is expressed as [12] $S_\zeta = \begin{cases} 1 & \text{if top switch is ON and lower switch is OFF} \\ 0 & \text{if top switch is OFF and lower switch is ON} \end{cases} \quad \zeta = \{a, b, c\}$ (19)

The voltage at point ζ w.r.t. neutral point N is

$$V_{\zeta N} = S_\zeta V_{dc}, \zeta = \{a, b, c\} \tag{19}$$

Denoting the phase delay of 120° as a constant $d = e^{j\frac{2\pi}{3}}$, the output voltage of the inverter (equivalently input to the stator windings) can be defined as space vector v_s:

$$v_{s,k} = \frac{2}{3} V_{dc} \left(S_a + dS_b + d^2 S_c\right) = \frac{2}{3} V_{dc}.D_k \quad k = 0, 1, ...7, \tag{20}$$

where $D_k = \left(S_a + dS_b + d^2 S_c\right)$

D_k represents two null vectors and six different unitary vectors placed at equidistant angular positions on a circle in a complex plane as explained in Figure 3 [10,11]. Null vectors are at the origin and are not shown. Based on a certain selection criterion, a specific switching state is chosen by the controller and desired voltage vector is generated to control stator flux, currents, and ultimately manipulating torque of the drive.

4. Proposed model predictive controller for dual induction motor drive

The proposed MPC for dual induction motor drive is shown in Figure 4. This design is based on the so-called predictive torque control (PTC) scheme introduced in [3].

As explained earlier, estimations of stator and rotor fluxes (ψ_{si} & ψ_{ri} $i = 1, 2$) are required at present sampling instant for predictive control. Stator fluxes of both motors are estimated using Kirchhoff's equations assuming a stationary reference frame [16]:

$$v_s = R_{s1} i_{s1} + \frac{d\psi_{s1}}{dt} \tag{21}$$

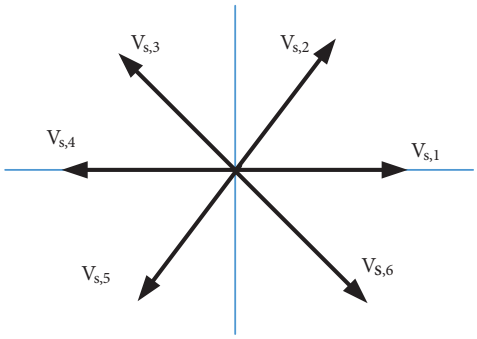

Figure 3. Voltage space vectors.

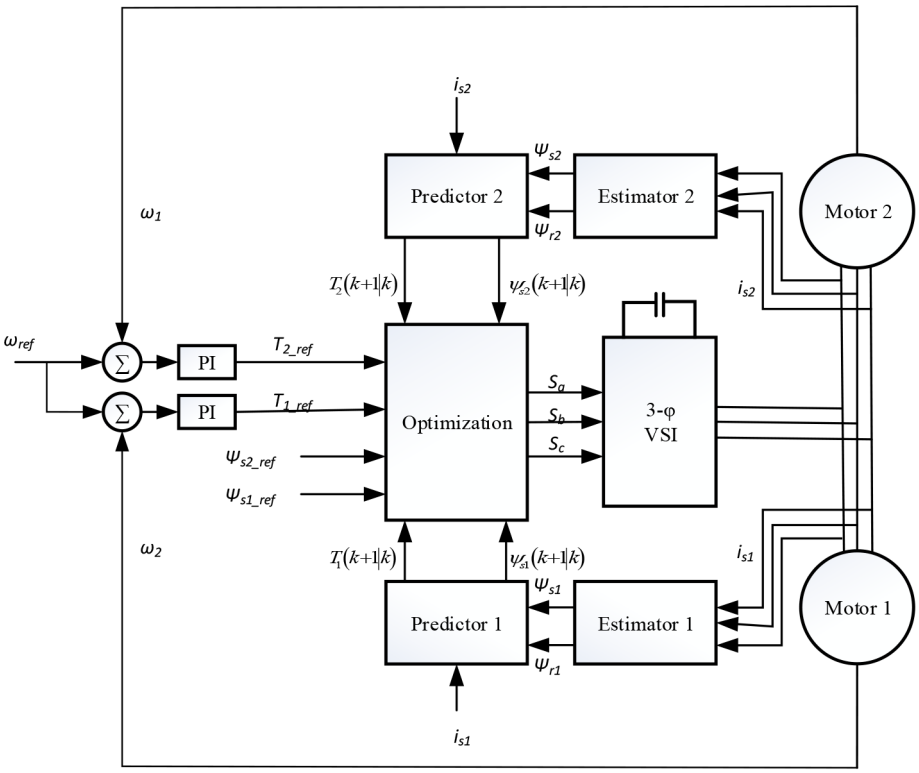

Figure 4. Proposed MPC controller for a dual induction motor drive.

$$v_s = R_{s2} i_{s2} + \frac{d\psi_{s2}}{dt} \tag{22}$$

For sampling time T_s, Euler's derivative approximation formula gives us the following discrete versions of the above equations to estimate stator fluxes [1,12]:

$$\hat{\psi}_{s1}(k) = \hat{\psi}_{s1}(k-1) + T_s\left(v_s(k) - R_{s1} i_{s1}(k)\right) \tag{23}$$

$$\hat{\psi}_{s2}(k) = \hat{\psi}_{s2}(k-1) + T_s\left(v_s(k) - R_{s2} i_{s2}(k)\right) \tag{24}$$

The next step in implementing PTC consists of obtaining predictions of the controlled variables (stator fluxes and torques) from the internal model of the system. Stator fluxes are predicted from the same equations used for estimation:

$$\psi_{s1}(k+1|k) = \hat{\psi}_{s1}(k) + T_s(v_s(k) - R_{s1}i_{s1}(k)) \tag{25}$$

$$\psi_{s2}(k+1|k) = \hat{\psi}_{s2}(k) + T_s(v_s(k) - R_{s2}i_{s2}(k)) \tag{26}$$

$\psi_s(k+1|k)$ represents the future value of stator flux at $k+1$, while this value is predicted at instant k using the internal model of the motor. Torque predictions are obtained from Eq. (10) directly:

$$T_1(k+1|k) = \frac{3}{2}pIm(\bar{\varphi}_{s1}(k+1|k)\, i_{s1}(k+1|k)) \tag{27}$$

$$T_2(k+1|k) = \frac{3}{2}pIm(\bar{\varphi}_{s2}(k+1|k)\, i_{s2}(k+1|k)) \tag{28}$$

As is evident from the previous equations, we also require current predictions to obtain torque predictions. Current predictions are evaluated using the state space model in (13) and (14):

$$i_{s1}(k+1|k) = \frac{\tau_{\sigma1}+T_s}{\tau_{\sigma1}}.i_{s1}(k) + \frac{T_s}{\tau_{\sigma1}+T_s}.\frac{1}{R_{\sigma1}}\left\{\left(\frac{k_{r1}}{\tau_{\sigma1}} - k_{r1}j\omega_1\right)\hat{\varphi}_{r1}(k) + v_s(k)\right\} \tag{29}$$

$$i_{s2}(k+1|k) = \frac{\tau_{\sigma2}+T_s}{\tau_{\sigma2}}.i_{s2}(k) + \frac{T_s}{\tau_{\sigma2}+T_s}.\frac{1}{R_{\sigma2}}\left\{\left(\frac{k_{r2}}{\tau_{\sigma2}} - k_{r2}j\omega_2\right)\hat{\varphi}_{r2}(k) + v_s(k)\right\} \tag{30}$$

Note that both torque and stator flux predictions are expressed in terms of inverter voltage $v_s(k)$; hence a total of seven predictions can be made for each controlled variable based on seven switching states $v_{s,k}$ for $k = 0, 1, 2...7$. The state that produces the minimum value of the cost function is applied on the next sampling instant.

The generalized structure of the objective function is given as

$$f_1 = \sum_{i=1}^{N} \|T_{ref1} - T_1(k+i|k)\|_{Q1} + \|\psi_{s\_ref1} - \psi_{s\_1}(k+i|k)\|_{R1} \tag{31}$$

$$f_2 = \sum_{i=1}^{N} \|T_{ref2} - T_2(k+i|k)\|_{Q2} + \|\psi_{s\_ref2} - \psi_{s\_2}(k+i|k)\|_{R2} \tag{32}$$

$$f = f_1 + f_2 + \sum_{i=1}^{N} \|i_{s1}(k+i|k) - i_{s2}(k+i|k)\|_S = f_1 + f_2 + \sum_{i=1}^{N} \|\Delta i_s(k+i|k)\|_S \tag{33}$$

The last term is included to minimize the difference between the two motor currents to avoid unbalanced condition without averaging the entire system. In this manner, a switching state is determined that not only tries to force both motors to follow their torque and stator references, but also maintains the stator current balance. R, Q, & S are weighting matrices and N represents the prediction horizon. In power electronics applications where sampling time is normally in microseconds, higher values of prediction horizon N pose computational complexities. For example in (33) if $N = 2$, there will 49 predictions for each error term, which will amount to 245 predictions in one sampling interval. This will require an ultrafast DSP processor for

real-time implementation and will create computational delays that affect the steady-state performance of the system. In finite control set model predictive control (FCS-MPC), the prediction horizon is usually taken as one [17]. The weighting factors Q and S are chosen as one and the only weighting factor to be tuned is R, which assigns relative importance to flux error and is normally chosen as the ratio between nominal values of torque and flux to assign them equal importance:

$$r = \frac{T_{nom}}{\psi_{nom}} \tag{34}$$

In FCS-MPC constraints are implemented as logical limits. A logical operator is used to trigger the limit. As an example consider the following amplitude limiting cost function:

$$g = |i_s^* - i_s\,(k+1)| + \eta\,(|i_s| > I_{\lim}) \tag{35}$$

It implements a constraint on the stator current i_s and the restricting value is defined as $I_{\lim}$, where constant η is taken as a large value. If the current is within the safe limits, i.e. the logic condition $|i_s| > I_{\lim}$ is "false", the cost function only involves the stator current error for optimization, i.e. $g = |i_s^* - i_s\,(k+1)|$. Whenever current crosses that limit, the logic condition $|i_s| > I_{\lim}$ becomes "true" and the cost function takes the form $g = |i_s^* - i_s\,(k+1)| + \eta$, which puts almost negligible emphasis on the current error due to the presence of a large constant and the inputs that caused this condition to occur are effectively excluded from the feasible set. To implement this constraint, (35) is added to (33) to modify the cost function.

5. Simulations and results

The proposed controller is simulated and compared with DTC for the single pole pair identical motors given in the Table. For a fair comparison between the two techniques, the same operating conditions are assumed. Practically, motors of the same specifications may differ within ±3% of their nominal parameter values. We will simulate the drive for mismatched characteristics assuming the worst case.

Table. Dual induction motor drive fed by a three-phase voltage inverter.

Parameter	Symbol	Value	Units
Sampling Time	T_s	40	μs
Moment of Inertia	J	0.0031	$Kg.m^2$
Stator Inductance	L_s	0.3419	H
Rotor Inductance	L_r	0.3513	H
Magnetizing Inductance	L_m	0.3240	H
Stator Resistance	R_s	3	Ω
Rotor Resistance	R_r	4.1	Ω
Nominal Stator Flux	ψ_{s_nom}	0.954	Wb
Nominal Torque	T_{nom}	9	$N.m$
DC Link Voltage	V_{dc}	160	$Volts$
Proportional Gain of PI controller	K_p	0.1	-
Integral Gain of PI Controller	K_i	0.05	-

Figure 5 shows the step responses for MPC and DTC of the ideal case when both the motors are 100% matched and unloaded. The MPC controller provides comparatively better transient response with no overshoot in the speeds and fast settling at the steady state value. There are, however, higher starting values of the phase

currents, which can pose a threat. As explained before, a logical condition can easily impose hard constraints on the initial current values to prevent damage. Similarly current distortion in MPC is observed to be 3% as compared to 8% in DTC. Figure 6 shows the torque and flux induced in the dual motors during the startup transience both for FCS-MPC and DTC. Again, MPC has faster dynamic response to DTC and less ripples are observed. DTC suffers from flux and torque ripples. Flux in both of the machines remains at the nominal values to avoid saturation. This is also observed for the torques.

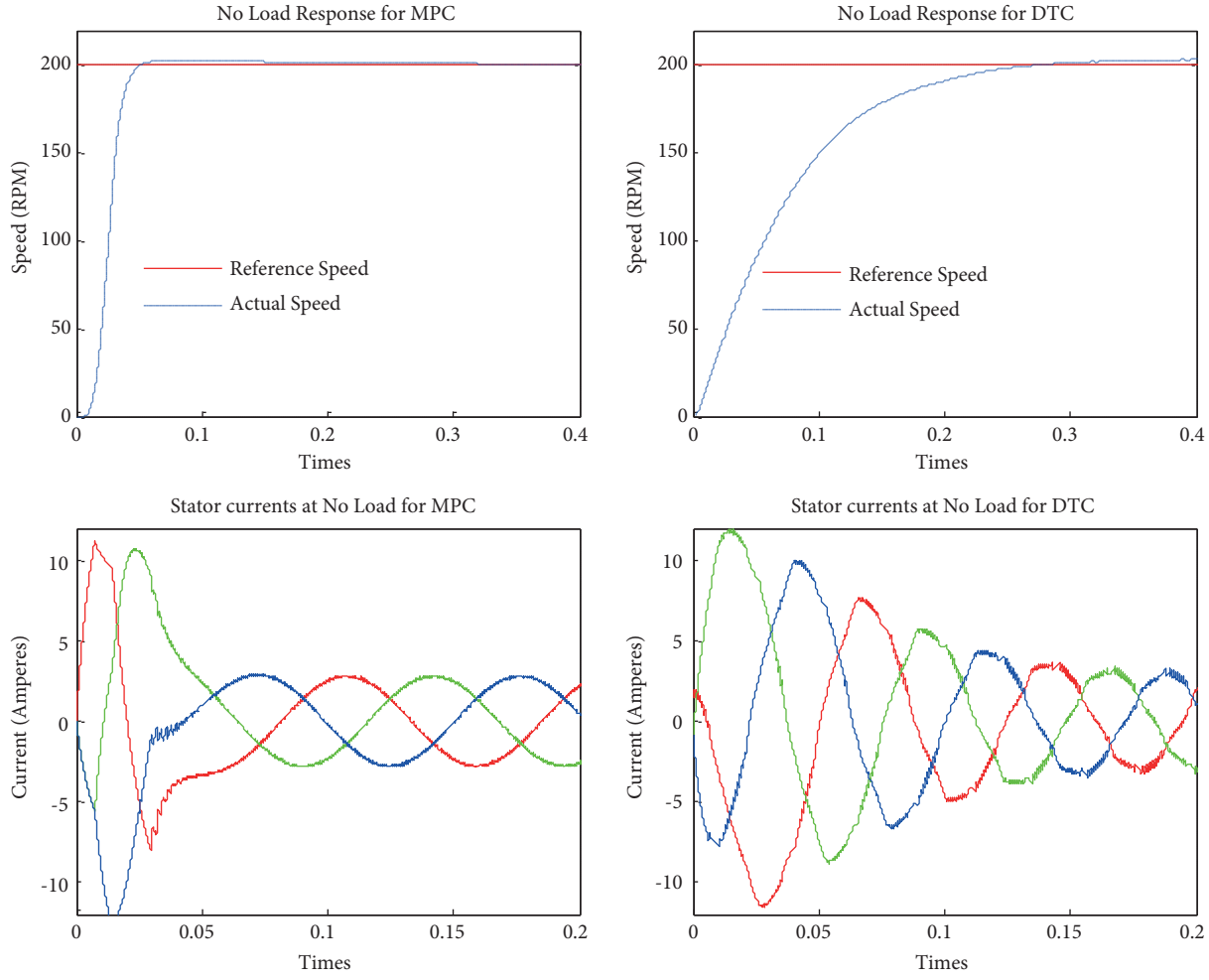

Figure 5. Step response of dual induction motors at no load condition: MPC and DTC response.

Figures 7 and 8 portray the situation when one motor is suddenly loaded and the current and load balance is disturbed. Motor 1 is applied with a load torque of 3 N.m at 0.5 s and a change in its speed is observed. The currents are perturbed momentarily; then the MPC controller tries to maintain the balance between them. Current transients and surges can be observed in the figure. Eventually, the speed of motor 1 is settled at a new value to balance the load torque and currents also settle at steady-state values once again. However, due to averaging, DTC is unable to maintain the current balance between the two motors (Figure 8). This unbalancing is also observed in flux response shown in Figure 9, where none of the motors is driven at rated flux and a higher torque ripple is also observed. MPC, on the other hand, keeps the dual operation separated and the effect of motor 1 saturation is not reflected in motor 2 flux, which tracks its nominal value as usual.

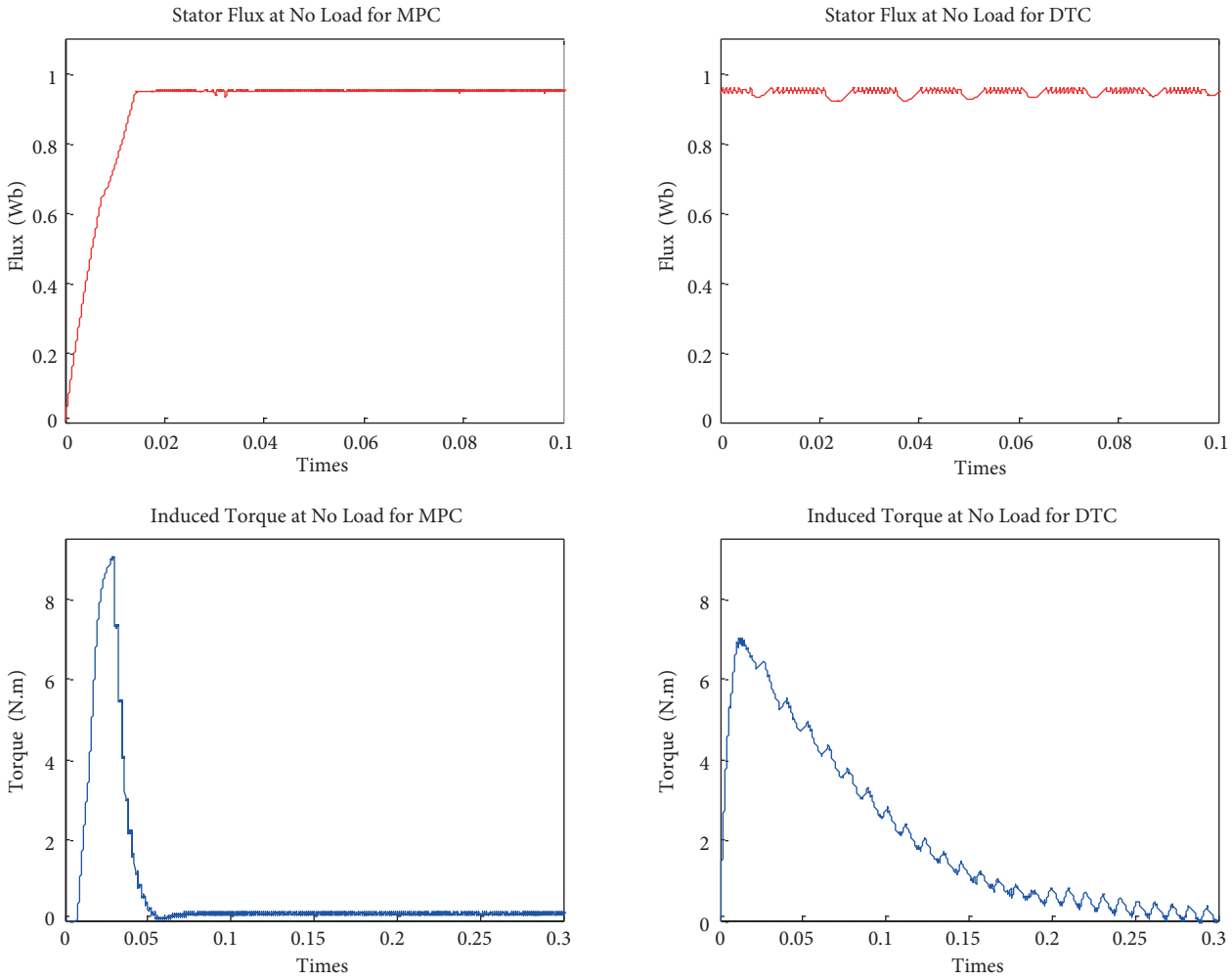

Figure 6. Torque and flux step response of motors at no load: MPC and DTC.

Another similar situation is depicted in Figure 10, which demonstrates the scenario of exchanging load between the dual induction motors. The figure shows that motor 1 is operating at a higher load than motor 2 (5 N.m and 3 N.m) and the load is exchanged between the motors at time 1.5 s. The motors go under transients and eventually settle at the steady states. When motor 1 is unloaded suddenly, its speed goes above the specified reference speed of 200 rad/s up to 220 rad/s; however, it settles down to nominal value within 0.5 s. Motor 2 gradually reduces its speed to balance the load torque shifted from motor 1. During this reduction, sinusoidal variations are observed that indicate that the controller is also trying to maintain the current balance. Motor 2 settles to a new speed within 0.5 s. This is, however, not the case with DTC, where no motor operates near the reference speed and torque ripple is much higher. DTC is also not able to effectively achieve current balance between the motors as explained earlier (Figure 8).

Practically two motors are never ideally matched. Figures 11 and 12 show the dynamic response of the drive both for MPC and DTC when the stator resistances of the two motors are mismatched. Resistance of motor 2 is 10% higher than that of motor 1. It is clear from the plots of MPC that a slight difference in the speeds is incurred due to resistance mismatching, which is further reduced by the MPC controller to achieve current balance. However, in DTC speeds are never restored to their reference values and current balance is

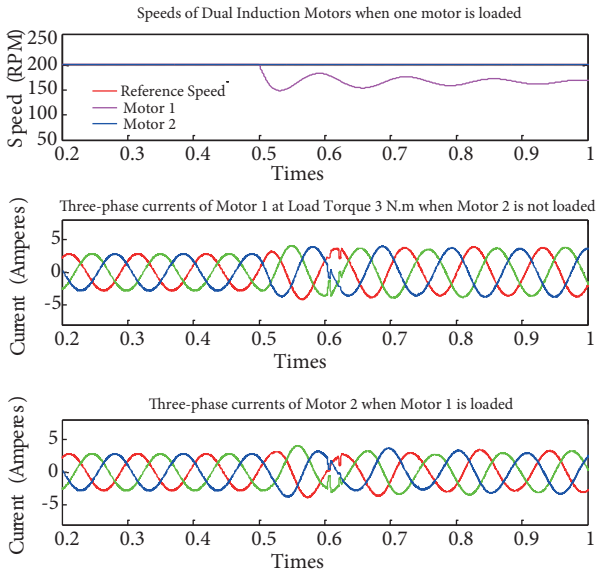

Figure 7. Speeds and currents of dual induction motors when one motor is loaded: MPC response.

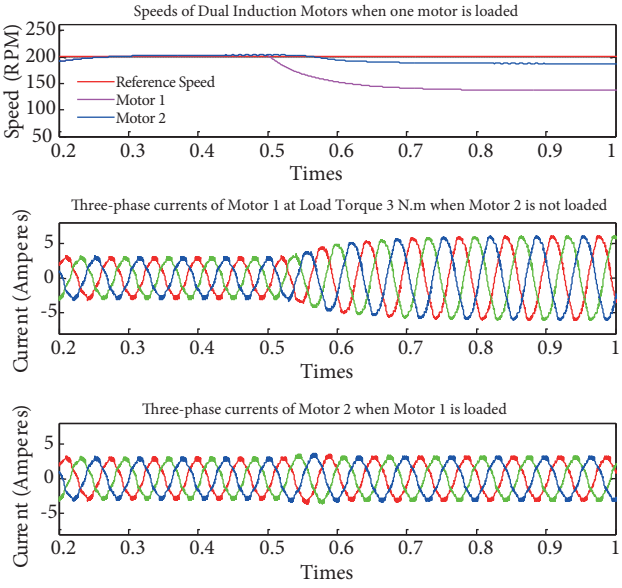

Figure 8. Speeds and currents of dual induction motors when one motor is loaded: DTC response.

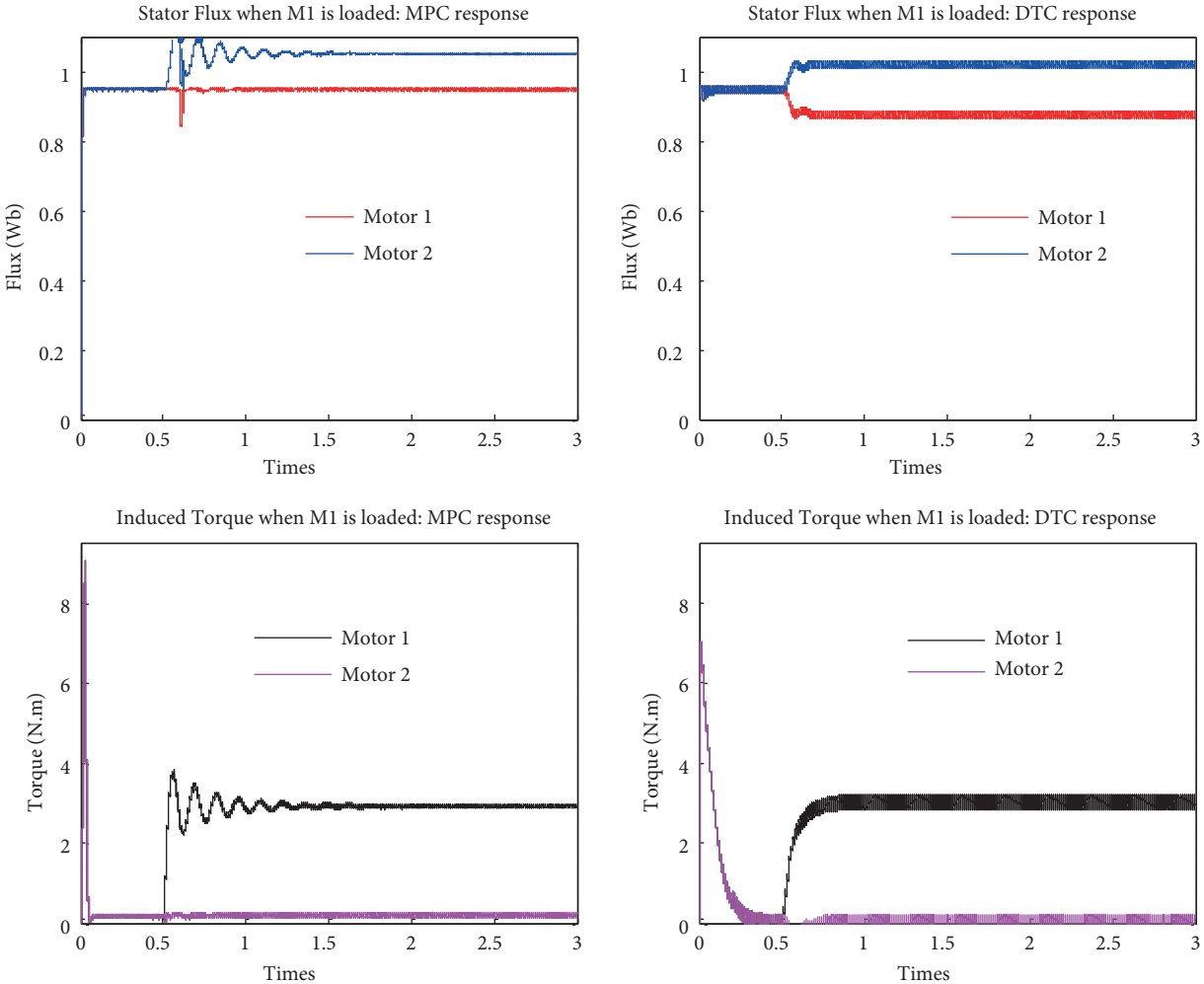

Figure 9. Torque and flux of dual induction motors when one motor is loaded: MPC and DTC.

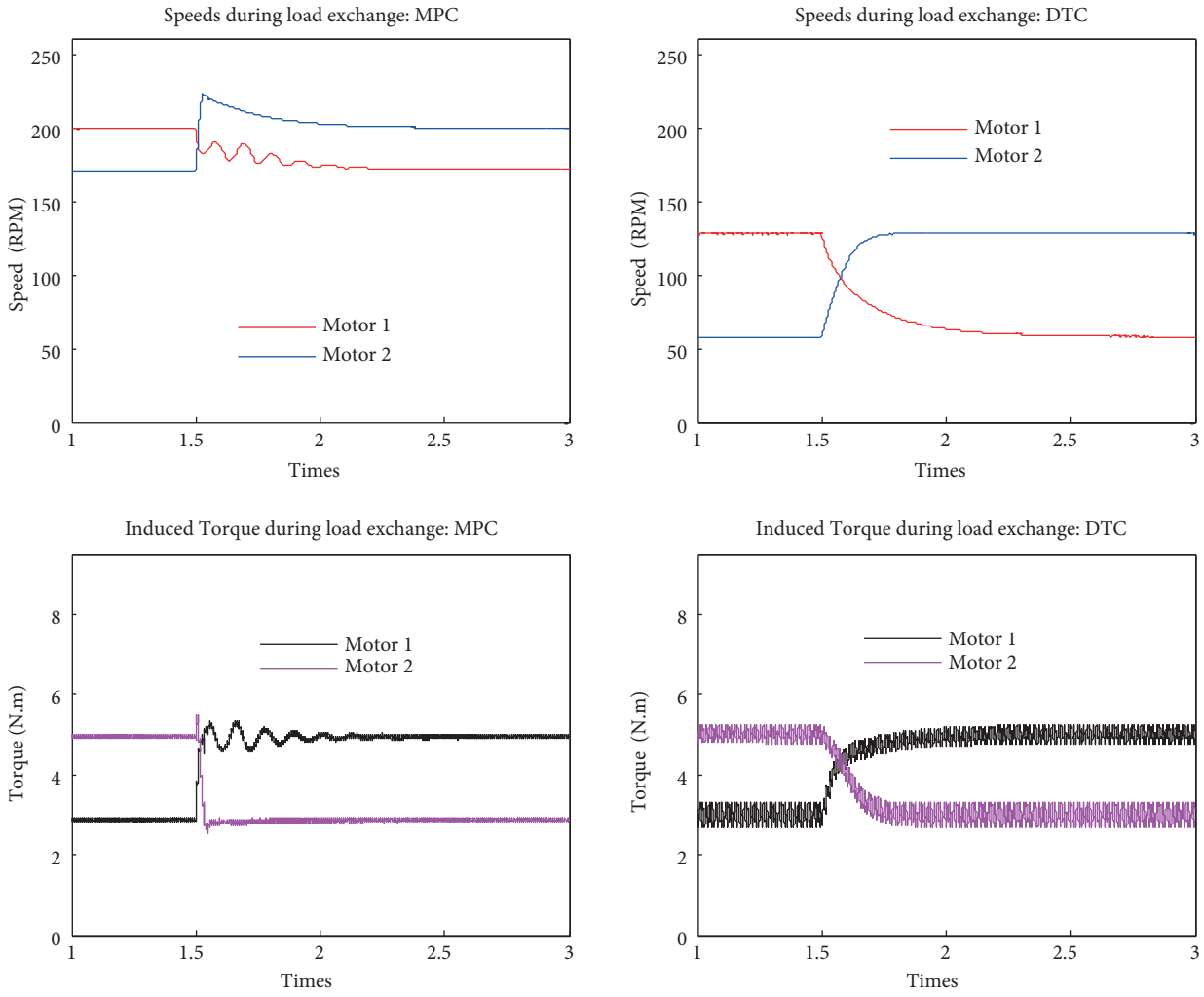

Figure 10. Speed and torque response during load exchange: MPC and DTC.

disturbed. Torque and flux response also indicate a slight difference of negligible importance for MPC but a higher torque ripple and unbalancing in fluxes for DTC.

Finally, Figures 13–15 show the situation when there is parameter mismatch in the stator resistances. A modelling uncertainty of 20% is also assumed in the MPC case. Usually, stator resistance increases with time due to heating and other factors but the model used by the MPC controller incorporates the constant value of this resistance. In short, stator resistance used by the controller to determine optimal control is not the actual resistance. This uncertainty is overcome by the controller in an effort to match the other variables such as currents and fluxes. A 20% stator resistance uncertainty is simulated and the results are presented in Figure 13. A mismatch of 5% between the two motors is also assumed. The plot shows that there is a slight difference between the two speeds due to mismatch and there is also overshoot and longer settling time due to uncertainty in resistances. However, these effects are sharply overcome by the controller and speeds and torques are driven back to their nominal values within 0.6 s. Figures 14 and 15 show various speed reversal plots for MPC and DTC under different parameter mismatches where slight deviations in speed tracking are observed. Results for various situations such as mismatched motors under load exchange, model uncertainties in other parameters,

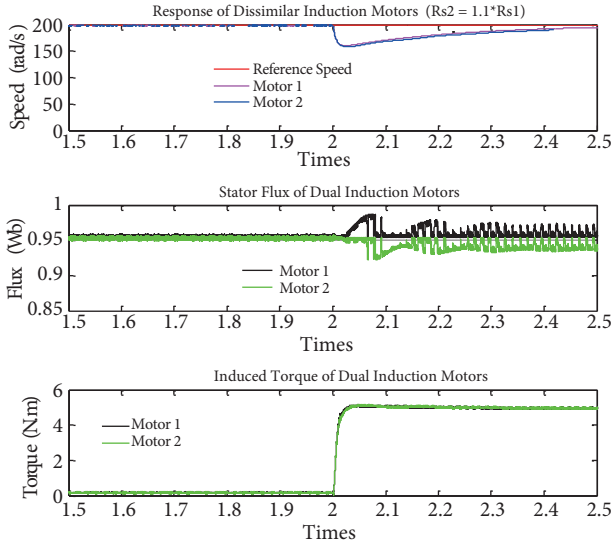

Figure 11. Speeds, flux and torque of dual induction motors when there is 10% mismatching in the stator resistance and both motors are loaded at $t = 2$ s: MPC response.

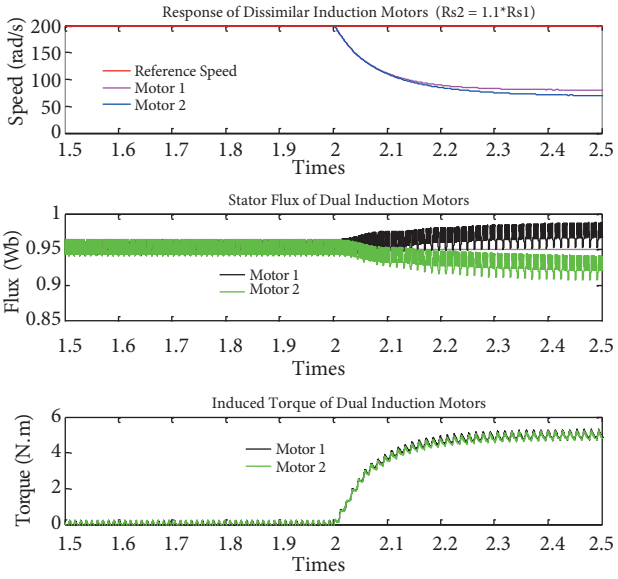

Figure 12. Speeds, flux and torque of dual induction motors when there is 10% mismatching in the stator resistance and both motors are loaded at $t = 2$ s: DTC response.

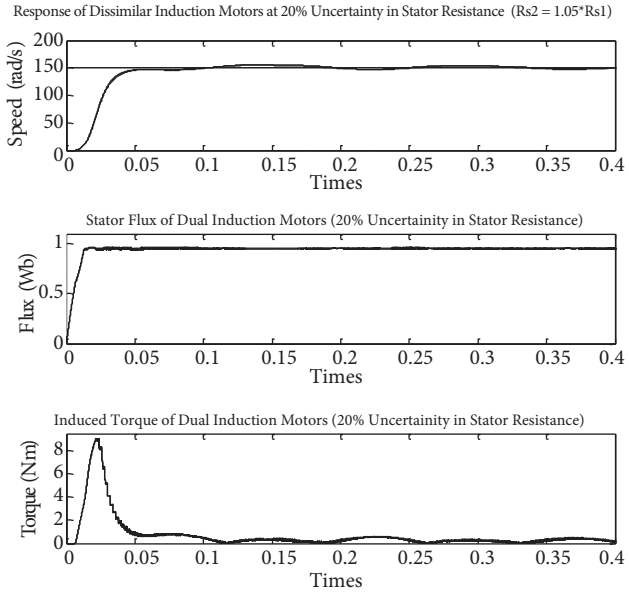

Figure 13. Response of motors when their stator resistances mismatch by 5%.

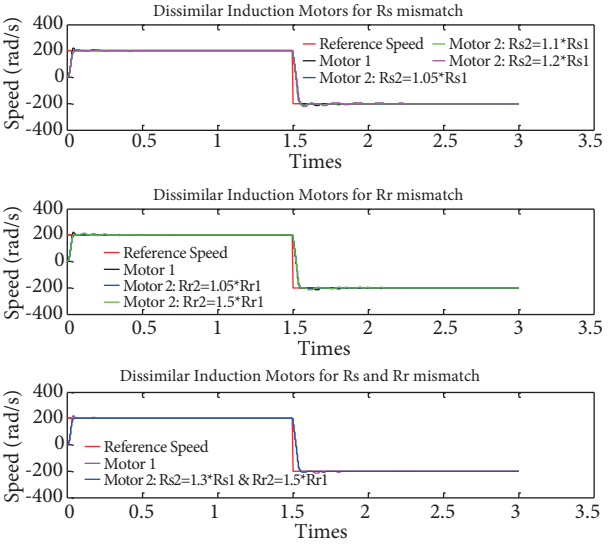

Figure 14. Parameter mismatching in stator and rotor resistances: MPC speed reversal.

mismatching in inductances, or rotor resistances also show satisfactory results and are omitted due to space constraints.

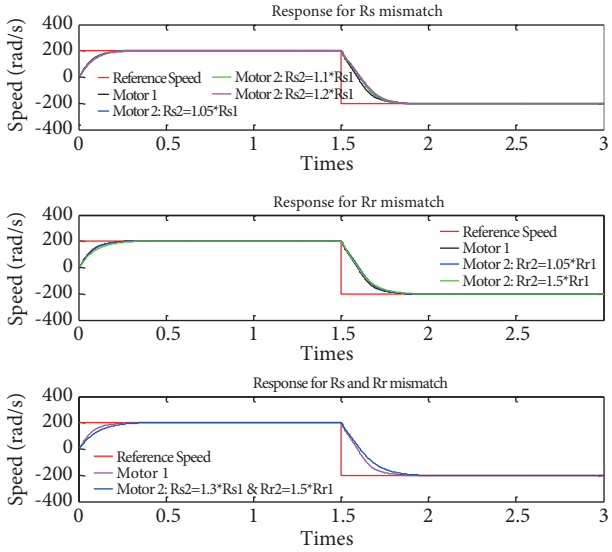

Figure 15. Parameter mismatching in stator and rotor resistances: DTC speed reversal.

6. Conclusion

The MPC controller proposed for a dual induction motor drive is compared with DTC under different operating conditions. It effectively handles dissimilar loads on the two fully matched and mismatched motors and keeps the controlled variables within the specified bounds and guarantees safe operation. A load exchange scenario is also efficiently treated without exceeding the nominal torques and entering into saturation of the stator windings. Dissimilarities in stator and rotor resistances and inductances create a slight difference between the controlled variables. Modelling uncertainties are simulated and better performance of MPC is observed. Cost function, however, is of complex nature and poses computational complications that can be further studied to reduce the effort by the digital target devices and improve delays. Incorporation of hard constraints to minimize initial currents will demand more computational resources. There are also no well-defined rules to determine weighting factors. These challenges could formulate the tasks to be investigated in the future.

Acknowledgments

The authors would like to acknowledge Universiti Teknologi Malaysia (UTM), the Islamia University of Bahawalpur (IUB), and Higher Education Commission (HEC) of Pakistan for providing financial support to conduct this research.

References

[1] Bose BK. Modern Power Electronics and AC Drives. Upper Saddle River, NJ, USA: Prentice Hall, 2002. pp. 333-435.

[2] Bose BK. Global energy scenario and impact of power electronics in 21st century. IEEE T Ind Electron 2013; 60: 2638-2651.

[3] Miranda H, Cortes P, Yuz JI, Rodriguez J. Predictive torque control of induction machines based on state-space models. IEEE T Ind Electron 2009; 56: 1916-1924.

[4] López M, Rodriguez J, Silva C, Rivera M. Predictive torque control of a multidrive system fed by a dual indirect matrix converter. IEEE T Ind Electron 2015; 62: 2731-2741.

[5] Ruxi W, Yue W, Qiang D, Yanhui H, Zhaoan W. Study of control methodology for single inverter parallel connected dual induction motors based on the dynamic model. 37th IEEE Power Electronics Specialists Conference; 18–22 June 2006; Jeju, South Korea. IEEE. pp. 1-7.

[6] Matsuse K, Kawai H, Kouno Y, Oikawa J. Characteristics of speed sensorless vector controlled dual induction motor drive connected in parallel fed by a single inverter. IEEE T Ind Appl 2004; 40: 153-161.

[7] Rodriguez J, Kazmierkowski MP, Espinoza JR, Zanchetta P, Abu-Rub H, Young HA, Rojas CA. State of the art of finite control set model predictive control in power electronics. IEEE T Ind Informat 2013; 9: 1003-1016.

[8] Brando G, Piegari L, Member S, Spina I. Simplified optimum control method for monoinverter dual parallel PMSM drive. IEEE T Ind Electron 2018; 65: 3763-3771.

[9] Wang J, Wang Y, Wang Z, Yang J, Pei Y, Dong Q. Comparative study of vector control schemes for parallel-connected induction motors. IEEE 36th Power Electronics Specialists Conference; 16 June 2005; Recife Brazil; IEEE. pp. 1264-1270.

[10] Gunabalan R, Sanjeevikumar P, Blaabjerg F, Ojo O, Subbiah V. Analysis and implementation of parallel connected two-induction motor single-inverter drive by direct vector control for industrial application. IEEE T Power Electron 2015; 30: 6472-6475.

[11] Mohktari H, Alizadeh A. A new multi-machine control system based on direct torque control algorithm. 7th International Conference on Power Electronics; 22–26 October 2007; Daegu, South Korea; IEEE. pp. 1103-1108.

[12] Han P, Cheng M, Chen Z. Dual-electrical-port control of cascaded doubly-fed induction machine. IEEE T Ind Appl 2017; 53: 1390-1398.

13 Lee Y, Ha JI. Control method for mono inverter dual parallel surface-mounted Permanent-Magnet Synchronous Machine drive system. IEEE T Ind Electron 2015; 62: 6096-6107.

[13] Rodriguez J, Pontt J, Silva CA, Correa P, Lezana P, Cortes P, Ammann U. Predictive current control of a voltage source inverter. IEEE T Ind Electron 2007; 54: 495-503.

[14] Correa P, Pacas M, Rodriguez J. Predictive torque control for inverter-fed induction machines. IEEE T Ind Electron 2007; 54: 1073-1079.

[15] Rodriguez J, Cortes P. Predictive Control of Power Converters and Electrical Drives. Chichester, UK: John Wiley & Sons, 2012. pp. 117-132.

[16] Davari SA, Khaburi DA, Wang F, Kennel R. Robust sensorless predictive control of induction motors with sliding mode voltage model observer. Turk J Elec Eng & Comp Sci 2013: 21: 1539-1552.